Inorganic Chemistry Communications 172 (2025) 113710

Contents lists available at ScienceDirect

Inorganic Chemistry Communications

journal homepage: www.elsevier.com/locate/inoche

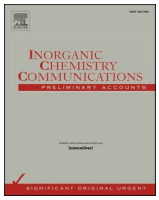

Short communication

Synthesis of low-content Mn-doped ZnO thin films: Characterizations and density functional theory studies

Elhadj Benrezgua [a,b,*], Rabie Amari [a,c], Ammar Boukhari [a,d], Djamel Allali [a,d], Smail Terchi [a,e], Abdelhamid Guellil [f], Bahri Deghfel [a,g], Abdelhalim Zoukel [h], Ahmad Azmin Mohamad [i,**]

[a] Laboratory of Materials and Renewable Energy, Faculty of Sciences, University of M'sila University Pole, Road Bourdj Bou Arreiridj, M'sila 28000, Algeria
[b] Department of Natural and Life Sciences, Faculty of Sciences, University of M'sila University Pole, Road Bourdj Bou Arreiridj, M'sila 28000, Algeria
[c] Department of Civil Engineering, Faculty of Technology, University of M'sila, Algeria
[d] Department of Mechanical Engineering, Faculty of Technology, University of M'sila, Algeria
[e] Department of Chemistry, Faculty of Sciences, University of M'sila, Algeria
[f] Department of Chemistry, Faculty of Sciences, University of Biskra, Algeria
[g] Department of Physics, Faculty of Sciences, University of M'sila, Algeria
[h] Laboratory Physico-Chemistry of Materials, Laghouat University, Laghouat, Algeria
[i] Energy Materials Research Group (EMRG), School of Materials and Mineral Resources Engineering, Universiti Sains Malaysia, 14300 Nibong Tebal, Pulau Pinang, Malaysia

ARTICLE INFO

Keywords:
Mn-doped ZnO thin films
DFT
LDA + U correction
Antiferromagnetic phase
Sol-gel method
Spin coating

ABSTRACT

This study aims to prepare manganese-doped zinc oxide (MZO) thin films with low Mn content (x = 0, 2, 4 %) using the sol–gel spin coating method and to characterize their structural, optical, and magnetic properties. Experimental techniques were complemented by Density Functional Theory calculations with Hubbard correction (DFT-LDA + U). All films exhibit a polycrystalline wurtzite hexagonal phase of ZnO. As the Mn doping increases, all diffraction peaks are getting weaker, which leads to deterioration in the crystallinity of the samples. Furthermore, Mn doping affects the grain size (57.44–38.20 nm), the surface morphology (rms: 45.24–30.47 nm), the transmittance (93–54 %) and the optical band gap energy (E_g: 3.27–3.18 eV). Photoluminescence spectra reveals ultraviolet peaks (386–395 nm) along with weak green (525 nm) and strong (438 nm) and weak (475 nm) blue peaks. DFT-LDA + U calculations exhibits an antiferromagnetic phase with slightly reduced E_g (3.379 eV for x = 0 % and 3.267 for 3.7 %), attributed to the influence of Mn3d states near the Fermi level. This study presents a comprehensive analysis of low-content Mn-doped ZnO thin films by combining experimental and theoretical approaches. The findings provide valuable insights into the electronic, structural, optical, and magnetic properties of MZO, emphasizing the critical role of Mn 3d states in altering the magnetic behavior and adjusting E_g.

1. Introduction

Zinc oxide (ZnO) stands out as a II–VI semiconductor material characterized by a direct wide band gap of 3.37 eV and a substantial exciton binding energy of 60 meV at room temperature. This unique combination of properties, including high chemical stability, non-toxicity, low growth temperature, and transparency in the visible range, makes ZnO a highly promising candidate for various applications and its potential spans across multiple devices.

Recent years have seen a surge in research focusing on the doping of ZnO with various elements such as Co, Mg, Al, Si, Ti, Ru and Mn to enhance its properties [1–4]. In particular, Mn has been frequently used as a dopant, with numerous studies investigating the diverse physical properties of Mn-doped ZnO (MZO) thin films synthesized under different experimental conditions [5]. This interest is driven by the potential of ZnO in developing optoelectronic devices in the blue and ultraviolet spectral ranges and its unique properties as a dilute magnetic semiconductor (DMS), including room temperature ferromagnetism and

* Corresponding author at: Laboratory of Materials and Renewable Energy, Faculty of Sciences, University of M'sila University Pole, Road Bourdj Bou Arreiridj, M'sila 28000, Algeria.
** Corresponding author.
E-mail addresses: elhadj.benrezgua@univ-msila.dz (E. Benrezgua), aam@usm.my (A.A. Mohamad).

https://doi.org/10.1016/j.inoche.2024.113710
Received 19 July 2024; Received in revised form 23 November 2024; Accepted 3 December 2024
Available online 6 December 2024

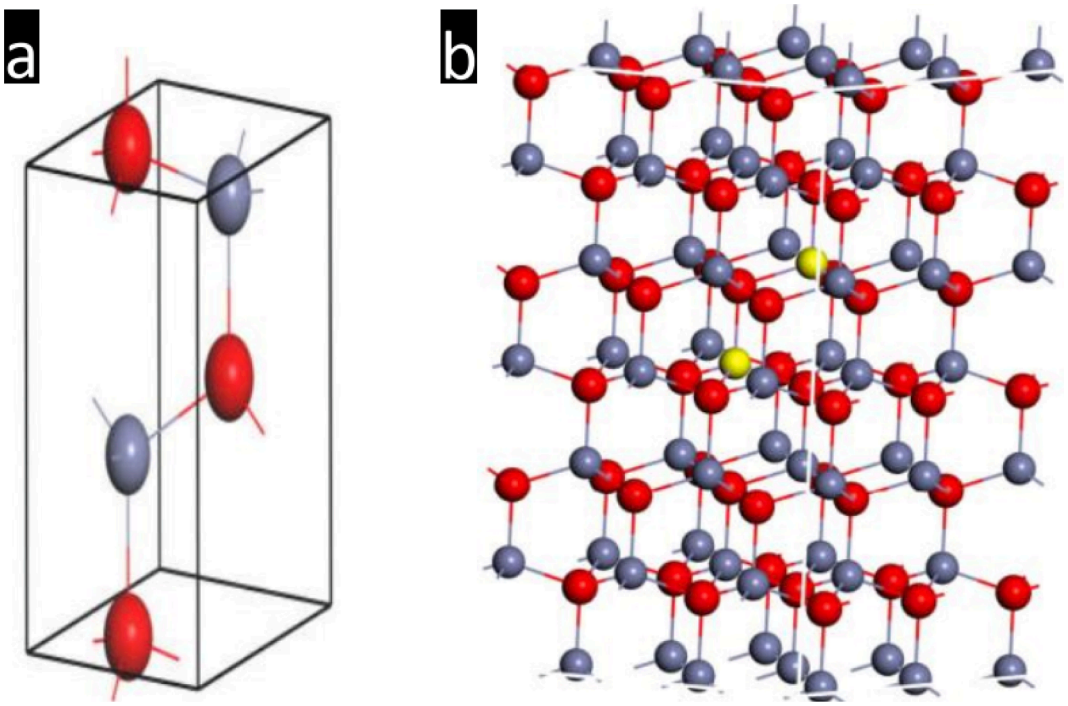

Fig. 1. The structure of ZnO-based material; (a) ZnO primitive cell, and (b) 3 × 3 × 3 ZnO supercell; two Mn atoms (yellow) substitute two Zn atoms (gray) to obtain a concentration of x = 3.7 %, and Zn atom is tetrahedrally surrounded by four O atoms (red).

semiconductivity [6]. These characteristics have drawn significant attention due to their magnetic, magneto-optic, and magnetoelectric attributes. On the other hand, theoretical predictions of the properties of ZnO and MZO structures have been conducted using first-principle pseudopotential methods based on density functional theory (DFT) with various exchange–correlation functionals [7,8]. Numerous DFT calculations using LDA or GGA have studied intrinsic and extrinsic point defects but face the band-gap problem, affecting energy difference accuracy [9]. DFT calculations with Hubbard correction (DFT-LDA + U or DFT-GGA + U) methods are proposed to correct formation and transition energy levels [9,10]. While DFT with pseudopotentials accurately predicts ground state properties, it struggles with *d* and *f* electron localization in transition materials [11]. The DFT-GGA + U approach significantly improves these calculations by better accounting for electron localization [12].

Numerous studies have been conducted on ZnO thin films covering a large Mn content and aiming to discover the phase transition for such materials [1,5,6]. Few experiments are limited to investigate low Mn doping which helps maintain the optical transparency, structural integrity, and electrical conductivity, while preventing defects and performance degradation associated with higher Mn levels in ZnO host lattice [13,14]. Besides, the study tackles challenges in DFT calculations related to accurately predicting the properties of MZO, especially for optical and electronic properties for materials that exhibit *d* and *f* electron localization, aiming to provide reliable computational models for optimizing ZnO-based devices [7–12].

This study aims to fabricate thin films of ZnO and MZO at low Mn concentrations (x = 2 and 4 %). Characterization of pure ZnO and MZO thin films was reported, with the electronic, structural, optical, and morphological properties comprehensively analyzed using various analytical techniques. Theoretically, the DFT-GGA + U approach was adopted to calculate the properties of ZnO and MZO structures. These theoretical predictions are then compared with experimental data.

2. Experimental and computational details

Manganese acetate tetrahydrate [$Mn(CH_3COO)_2{\cdot}4H_2O$], Zinc acetate dihydrate [$Zn\ (CH_3COO)_2{\cdot}2H_2O$] and isopropanol were used as a starting material, dopant source and stabilizer, respectively, to prepare MZO thin films by sol–gel method spin coated on glass substrates [15]. The metal ion concentration was set at 0.7 M with a 1:1 M ratio of Monoethanolamine (MEA) to metal ions, followed by stirring at 65 °C for 2 h and aging at room temperature for 24 h. The solution was dropped into a clean (ultrasonic cleaner and deionized water) and dry substrate at 2800 rpm for 30 s, followed by the preheating of the obtained films at 250 °C for 10 min. The preheating and coating process was repeated several times. The films were finally annealed at 500 °C for 1.5 h. The precursors were mixed in varying molar ratios to achieve the desired Mn dopant content, following the procedure detailed in Ref. [16].

Many techniques were used to investigate the films; X-ray diffractometer XRD (X'Pert PRO MPD-Cu-kα: λ = 1.5406 Å), Atomic Force Microscopy (AFM: MFP-3D CAR), Photoluminescence spectrofluorometer (PL: Perkin Elmer LS-50B λ = 325 nm) and Ultraviolet–visible spectrophotometer (UV–vis: UV-3101 Shimadzu). The film thicknesses were measured using Stylus Profilometer (model: D 500).

DFT calculations, as implemented in CASTEP code, were performed to estimate the electronic, structural, magnetic and optical properties of ZnO and MZO [17]. The exchange–correlation function was described using the generalized gradient approximation (GGA) in the scheme of Perdew–Burke–Ernzerhof (PBE) [18]. The substitutional method and the optimized ZnO primitive cell (Fig. 1.a) were used to constitute 3 × 3 × 3 ZnO supercell model (Fig. 1.b) and achieve the Mn content *x* of 3,7% [19]. The energy cut-off of 400 eV was used for the plane-wave ultrasoft pseudopotential method [20]. K-point meshes of 2 × 2 × 1 is used to sampling the Brillouin zone. The valence-electron configurations for the O ($2s^2\ 2p^4$), Zn ($3d^{10}\ 4s^2$) and Mn ($3d^5\ 4s^2$) were selected. The convergence tolerance is fixed at 0.05 eV/Å for maximum force, 5×10^{-6} eV/atom for energy change, 10^{-3} Å for maximum displacement and 0.05 GPa for maximum stress, 5.0 10^{-6} eV per atom for self-consistent field (SCF) threshold. The effective Hubbard U values within the semiempirical LDA + U approach were fixed at 8.0 eV for *O 2p,* 5.5 eV for Zn *3d*, and 10 eV for *Mn 3d* states [8,21,22]. Antiferromagnetic phase of MZO, supported by previous studies, was adopted [8,23].

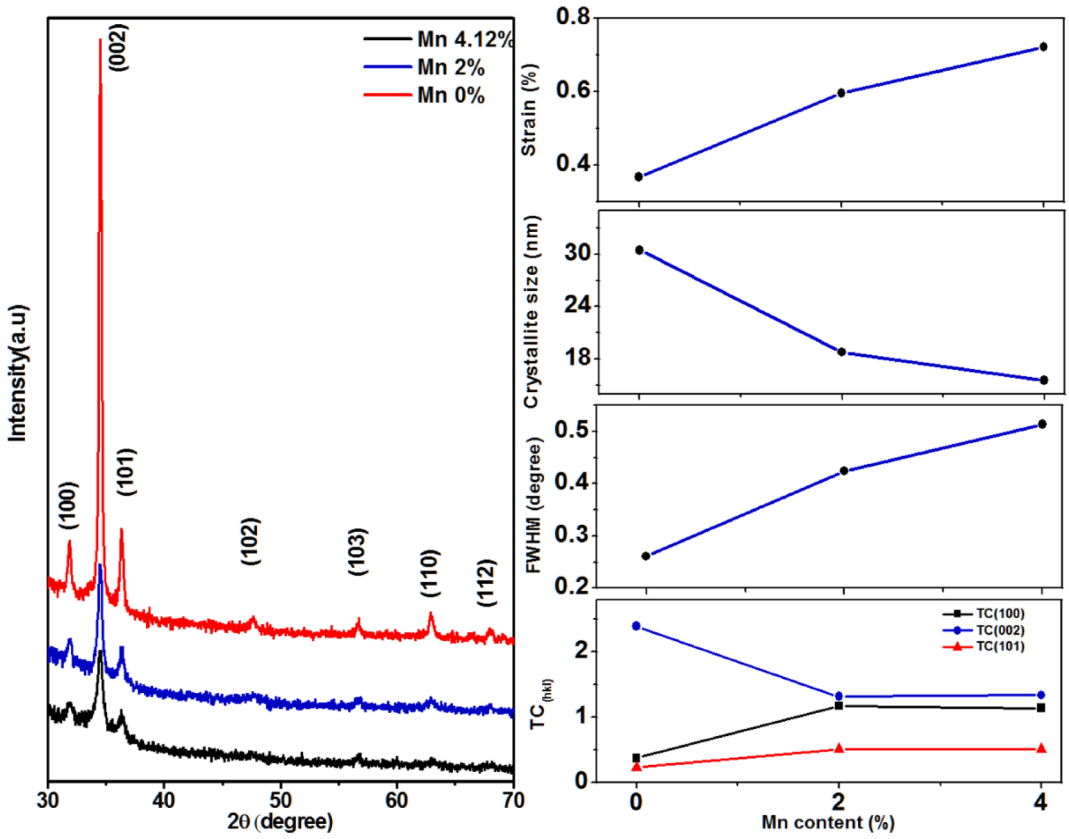

Fig. 2. (a) X-ray diffraction patterns, (b) Variation of strain, (c) Variation of crystallite size, (d) Variation of FWHM and (e) Variation of $TC_{(hkl)}$ of MZO thin films (x = 0, 2 and 4 %).

Table 1
Morphological and structural parameters of ZnO and MZO thin films (x = 2 and 4 %).

X (%)	2θ (°)	a = b (Å)	c (Å)	FWHM (°)	Peak intensity	Crystallite size (nm)	Grain size (AFM) (nm)	*Rrms* (nm)
0	34.459	3.244	5.198	0.251	(0 0 2)	32.00	57.44	45.24
2	34.455	3.245	5.204	0.425	(0 0 2)	19.02	36.67	29.48
4	34.453	3.245	5.205	0.501	(0 0 2)	15.01	38.20	30.47

3. Results and discussion

3.1. Experimental results

The XRD pattern (Fig. 2.a) validates the formation of a poly-crystalline wurtzite hexagonal phase for MZO thin films (x = 0, 2, and 4 %) without other phases. Furthermore, all samples exhibit a preferential orientation along the (0 0 2) axis as reported previously in the literature for MZO [5,8,24]. However, with increasing Mn doping, the diffraction peaks gradually weaken, indicating a decline in the crystallinity of the samples.

The lattice constants $a = b$ and c are found slightly affected by x due to the close ionic radius of Mn^{2+}, 0.83 Å, to that of Zn^{2+}, 0.74 Å (Table 1). The lattice strain ε and the average crystallite size (D) were estimated based on the methodology outlined in Ref. [25]. Unlike previous reports where excess Mn accumulates at grain boundaries at high doping levels [8,26], the strain value increases with x (Fig. 2.b), indicating the films become stressed due to the substitution of Zn^{2+} by Mn^{2+} cations. The crystallite size decreases with increasing x (Fig. 2.c) due to the strain caused by the incorporation of the dopant Mn^{2+} preventing grain growth [8,19,27].

The texture coefficient ($TC_{(hkl)}$) values were also estimated from the XRD pattern [25] and presented in Fig. 2.e. All films exhibit highest TC values and greater than unity for (0 0 2) plane indicating a better crystallinity and preferred growth along c-axis is slightly decreased with increasing x.

AFM images (1.0 × 1.0 μm^2 2D and 3D) are shown for ZnO and MZO thin films (Fig. 3a, b, c). The grains are round shaped with the average size decreasing with x (Table 1). This finding aligns with the decrease in (0 0 2) preferential orientation and then the c-axis grain growth as x increases. The surface becomes smooth with increasing level of x. This morphology is consistent with the values of the average grain size (Table 1) and the previous results reported by Amari et al. [19].

The increase in strain and reduction in grain and crystallite size with Mn doping enhance the density of grain boundaries, which are beneficial for photocatalysis and gas-sensing applications by increasing surface reactivity. Additionally, these changes can improve the electronic properties of the material, making it suitable for optoelectronic devices [6,14].

Fig. 4.a shows the transmission spectra of MZO thin films, which were used to deduce Eg (inset in Fig. 4.a). The transparency of the films generally decreases (93, 68 and 54 % for x = 0, 2 and 4 %, respectively) due to the increase in grain boundary density caused by the decrease in grain size with Mn doping. This decrease in transmission can be assigned to the loss of light due to oxygen vacancies [28]. The sharp UV absorption edge shifts slightly to longer wavelengths with increased Mn content, reducing Eg from 3.27 eV to 3.18 eV, which aligns with the findings reported for MZO film [15,26,29,30].

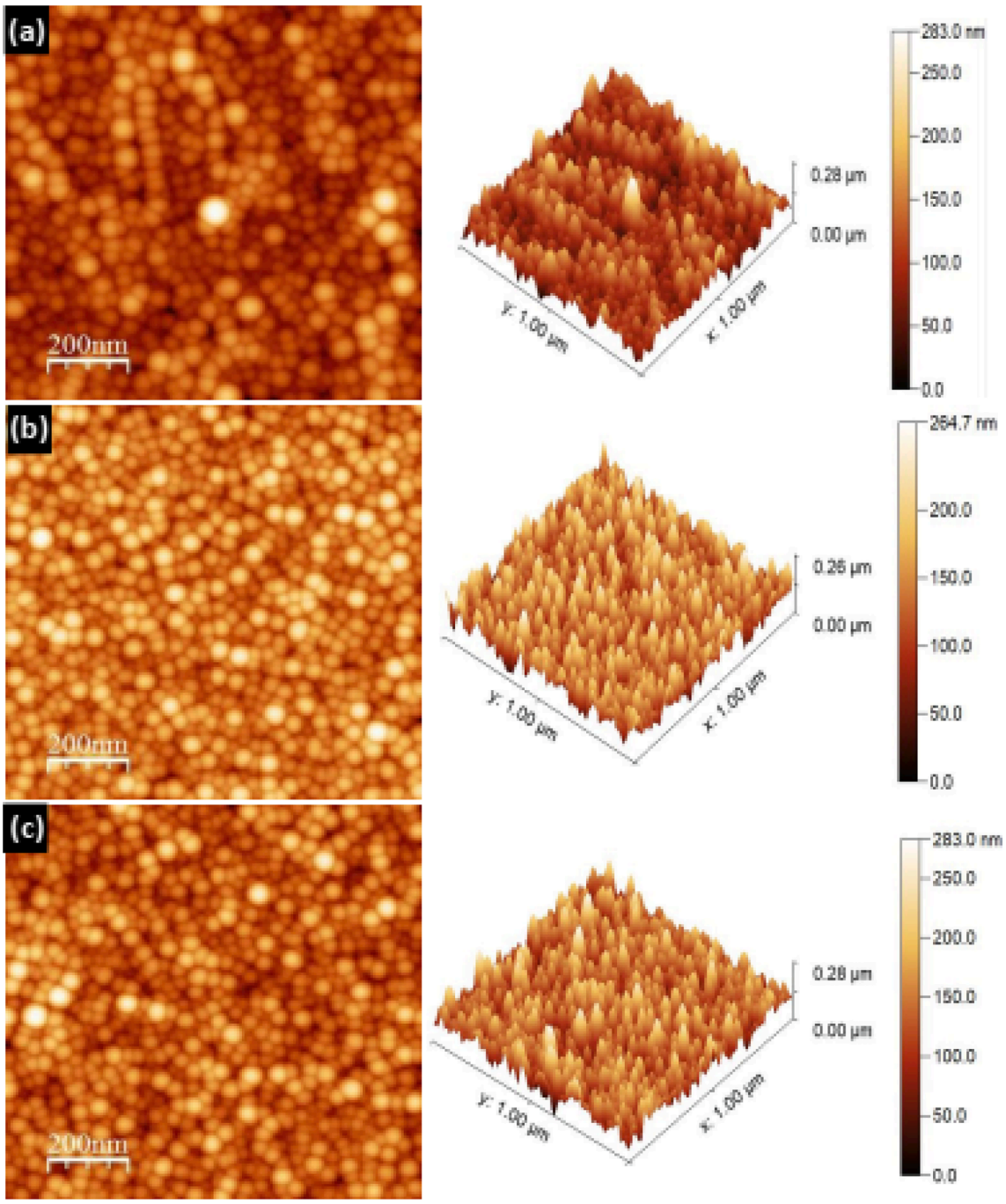

Fig. 3. AFM images of 1.0 × 1.0 μm^2 2D and 3D for (a) ZnO and MZO thin films (b) 2 % and (c) 4 % Mn content.

The optical parameters such as the absorption coefficient α, the extinction coefficient k, the refractive index n, the real part of the dielectric function and the imaginary part ε_2 were calculated using the measured film thickness (~242 nm), which was found to be unaffected by Mn doping, as well as the transmittance and the absorbance [31,32]. These parameters are presented for MZO thin films (Fig. 4.b, c, d). The straight line fitting of the factors $1/(n^2\text{-}1)$ versus the squared photon energy (E^2) [33] (inset in Fig. 4.c), enable us to estimate the static refractive index n_0, the dispersion energy E_d, the average oscillator energy E_o, the Urbach tail energy Eu and the static dielectric constant ε_o (Table 2).

The increase in the Urbach tail with a decreasing optical band gap (Table 2) is mainly due to disorder, defects, and localized states near the band edges. As the band gap narrows, defects like impurities and grain boundaries contribute to a higher density of states, broadening the absorption spectrum and extending the Urbach tail deeper into the forbidden gap [34–36].

The refractive index and the dielectric function increase with energy of the visible light and is affected by x due to the decrease in the crystallite size (Table 1). The absorption coefficient remains constant with increasing incident energy up to a certain point in the visible range, after which it shifts to lower energy and increases sharply with Mn doping, indicating a decrease in Eg. This decrease in E_g is common when dealing with thin film of ZnO [31,37,38] and MZO thin films [26,29,30]. The reduced transparency and band gap, along with increased refractive index, enhance light absorption, making the films suitable for photovoltaics, photocatalysis, and optoelectronic devices [14,39].

To identify the point-defect types, the photoluminescence (PL)

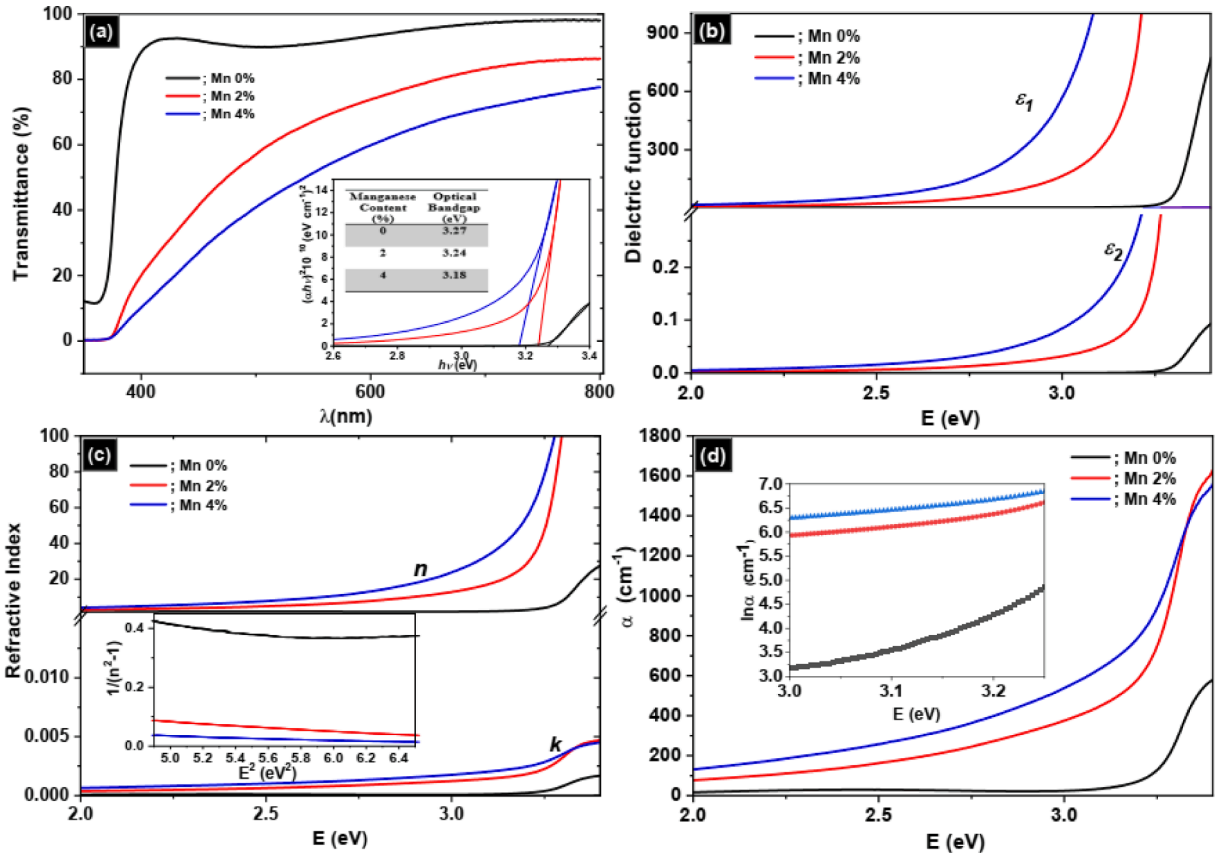

Fig. 4. (a) Optical transmission spectra, (b) dielectric function, (c) complex refractive index and (d) absorption coefficient of ZnO and MZO thin films ($x = 2$ %, 4 %,). Inset in (a) shows $(\alpha h\nu)^2$ versus $h\nu$ and Eg. Inset in (c) shows $1/(n^2\text{-}1)$ versus E^2. Inset in (d) shows ln(α) versus photon energy.

Table 2
Optical parameters of pure and MZO wurtzite structures ($x = 2$ %, 4 %).

x (%)	Dispersion energy E_d (eV)	Single-oscillator energy E_{osc} (eV)	Static dielectric constant ε_o (refractive index n_o)	Urbach tail energy Eu (eV)
0	7.57	4.23	2.79 (1.67)	0.153
2	11.54	2.76	5.18 (2.28)	0.393
4	25.87	2.72	10.51 (3.24)	0.475

spectra of MZO thin films are depicted (Fig. 5). The intensity of the NBE emission peak, assigned to the recombination of free exciton [25], increases and shifts slightly from 386 nm to 395 nm as Mn concentration increases. Furthermore, the intensity of PL increases with x, which is supported by previous works [26,40]. The emission at 411 nm, linked to electron transitions from interface traps to the valence band, appears with Mn doping [5]. The blue emission at 438 nm likely comes from interstitial zinc interstitial state (Zn_i) to the valence band (VB) transitions, the blue emission at 475 nm from oxygen vacancy (O_V) to valence band (VB) transitions, and the green emission at 525 nm from conduction band (CB) to oxygen zinc antisite level (O_{Zn}) transitions [25].

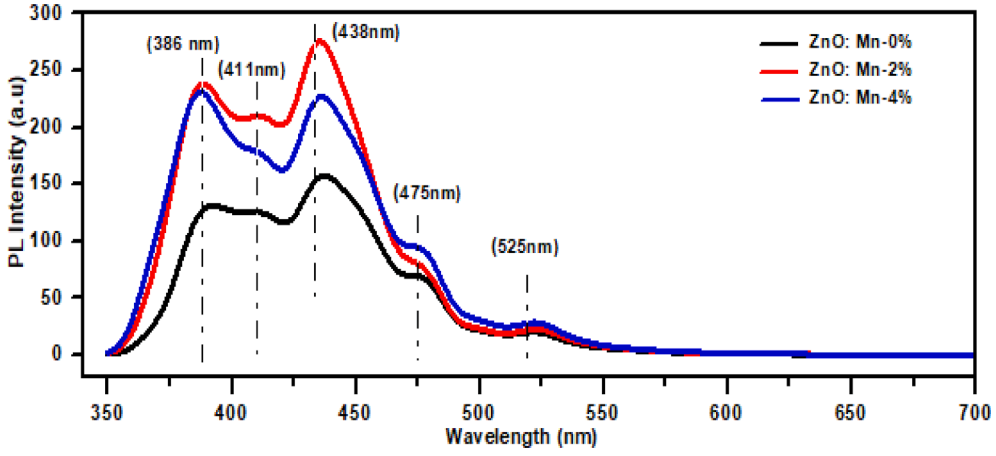

Fig. 5. PL spectra of 0%, 2% and 4% MZO thin films.

Table 3
Average Mulliken atomic, bond populations, effective valence, lattice constants and bond length of ZnO and MZO wurtzite structures ($x = 3.7$ %).

x (%)	Atomic Population (e)			Effective valence (e)		Bond Population (e)		Bond length (Å)		Lattice constants (Å)	
	Zn	Mn	O	Zn	Mn	Zn-O	Mn-O	Zn-O	Mn-O	$a = b$	c
0	0.952	–	−0.953	1.048	–	0.410	–	1.9719	–	3.237	5.237
3.7	0,954	0.957	−0.954	1.046	1.043	0.411	0.342	1.9738	2.1106	3.248	5.217

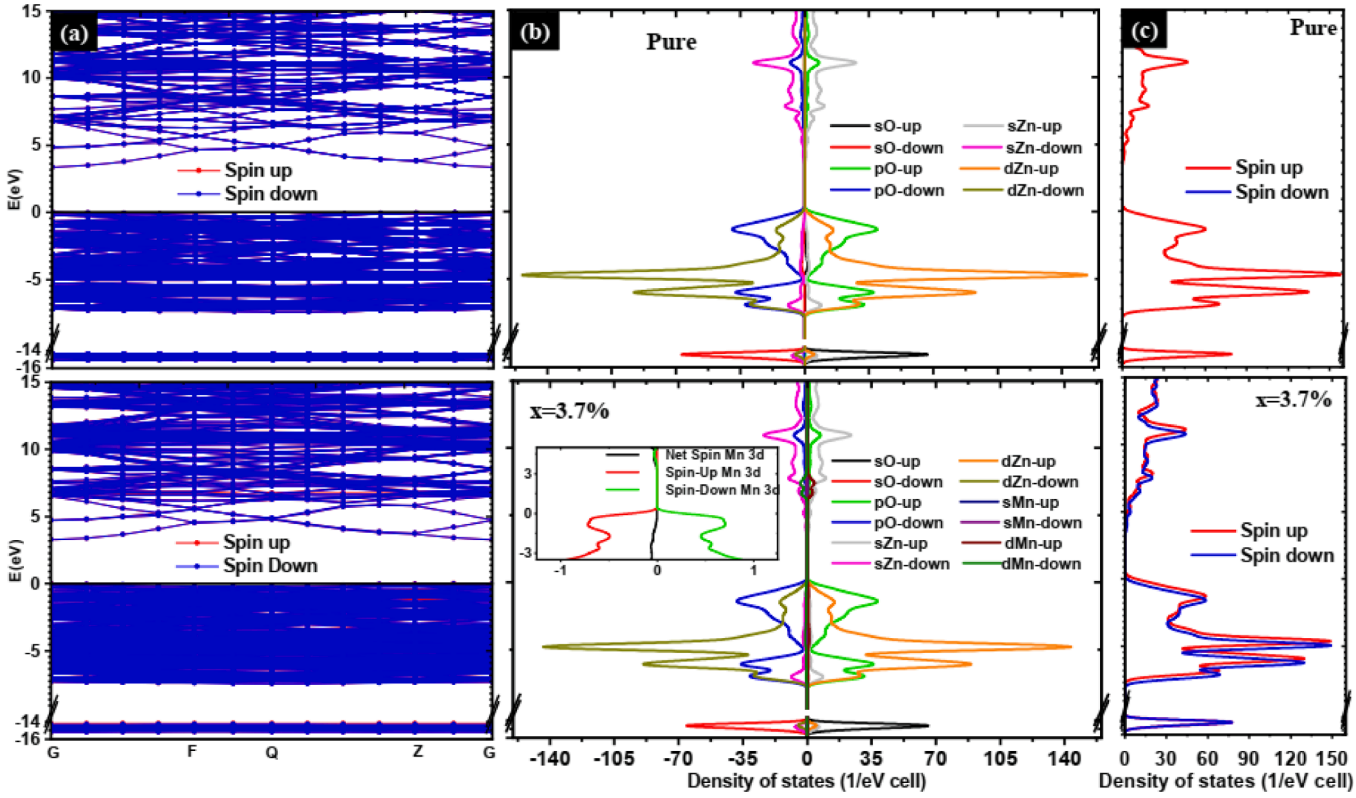

Fig. 6. (a) Band structures spin up (red) and spin down (blue), (b) PDOS of Zn 4s, Zn 3d, Mn 4s, Mn 3d, O 2s and O 2p states, and (c) total density of states of ZnO and MZO ($x = 3.7$ %). Inset in PDOS exhibits Mn 3d net spin states near Fermi level for MZO.

3.2. *DFT + U calculations*

In the ZnO host lattice, configuration where Mn ions are positioned in close proximity to O atom result in a stable state [8]. Furthermore, the Hubbard correction U significantly enhances the calculated energy gap (*Eg*). For this simulation, the effective Hubbard U values were fixed at 5.5 eV for Zn *3d* states, 10 eV for *Mn 3d* states and 8 eV *for O 2p* states [41].

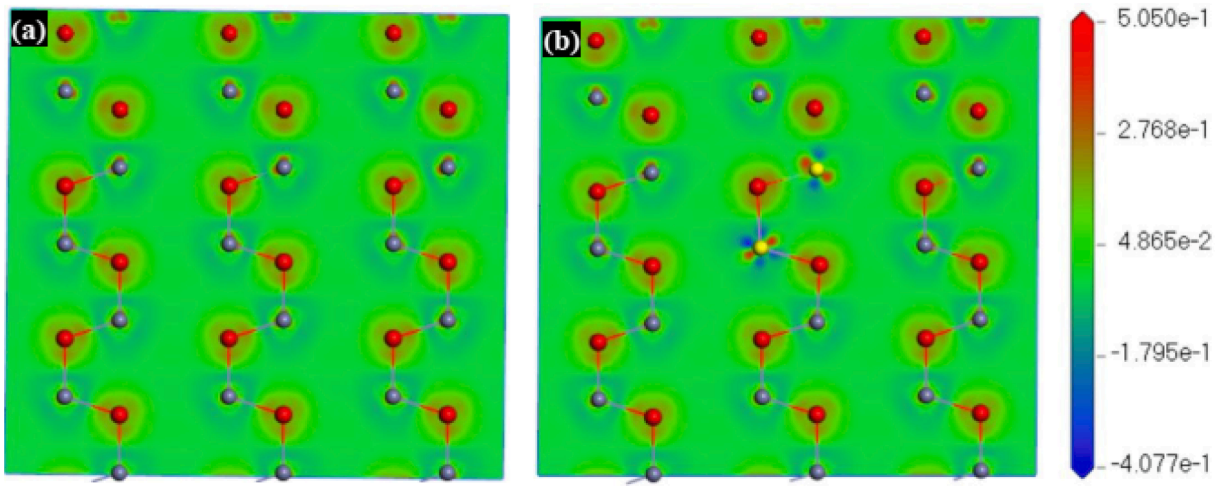

Fig. 7. Charge density difference distribution of (1 1 0) surface for (a) ZnO and (b) MZO structures.

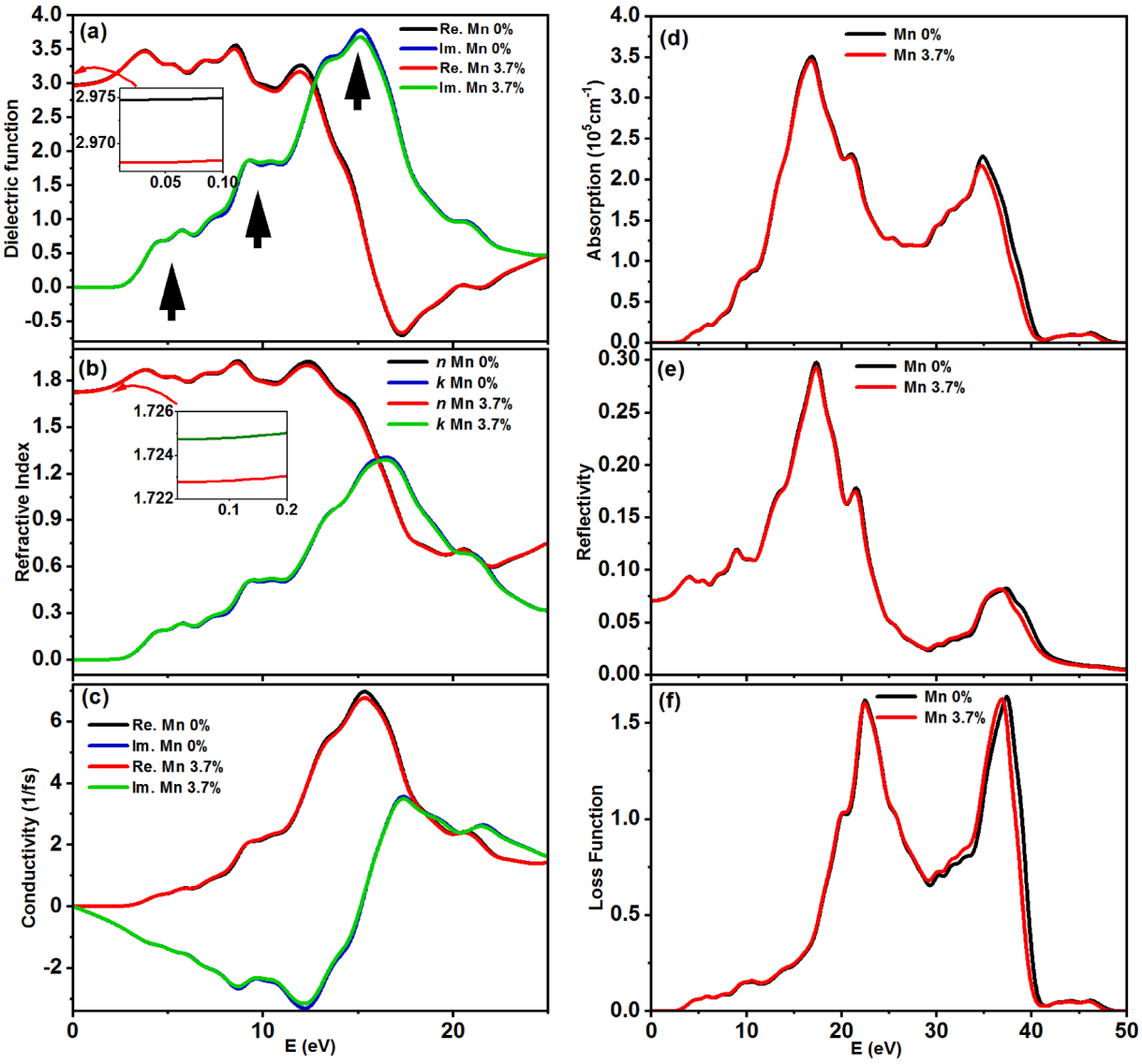

Fig. 8. Optical properties versus energy (E); (a) Complex dielectric function with inset exhibits the evolution of real part (ε_1)), (b) complex refractive index with inset shows the refractive index *n* for lower E), (c) complex conductivity function, (d) absorption coefficient, (e) optical reflectivity and (f) energy-loss function for ZnO ZnO and MZO (x = 3.7 %).

The lattice constants (a = b, c) are slightly decrease with increasing *x* (Table 3) and agree well with the experimental results (Table 2), with a relative error of 0.22 % for a = b and 0.75 % for c. The bond length changes slightly by Mn doping due to the similar atomic sizes of Zn and Mn atoms.

The theoretical band gap findings (3.379 eV for x = 0 and 3.267 for 3.7 %) align well with the experiment, showing a maximum relative error of only 3.3 %, with a direct Eg observed for both ZnO and MZO (Fig. 6(a)). The Mn doping leads to Eg narrowing where the top of the VB is primarily originated from Mn *3d* states (Fig. 6(b)). This Eg narrowing, attributed to sp-d exchange interactions and defect states introduced by Mn doping, has also been noticed in previous works [8,19].

The partial density of O 2s, O 2p, Zn 4s, Zn 3d, Mn 4s and Mn 3d, spin down and up states (PDOS) (Fig. 6(b)) and the total density of states (TDOS) (Fig. 6(c)) for ZnO and MZO are presented. The VB states, extended down to −8 eV and followed by a narrow band at around −15 eV, is primarily composed of a strong mixture among the O2p and Zn3d states and some contribution from the Mn3d states for MZO. The slight downward shift of the CB, dominated by Zn4s and Mn3d states (Inset in Fig. 6(b)), causes the decrease in *Eg* with *x*. Mn3d states are distributed around Fermi level with zero net spin leading to the antiferromagnetic phase of MZO. Mn doping produces a magnetic moment of about 1 μ_B/Mn with a negligible amount from its neighboring O atom. The antiferromagnetic phase configuration results in a zero net spin [42].

The charge density difference for slices of (1 1 0) surface containing Zn, O and Mn atoms for ZnO (Fig. 7.a) and MZO (Fig. 7.b) are shown. Red color indicates a charge accumulation around O, yellow color refers to the minimal difference and green color represents the charge loss around Zn or Mn. The high electronegativity of an atom correlates with its tendency to attract more electrons, as seen in the values for Zn (1.7), Mn (1.6), and O (3.5), which agrees with the bond populations and the average Mulliken atomic (Table 3). The degree of the mix of ionic and covalent bonding in ZnO and MZO is indicated by the difference between the effective valence charge and the formal ionic charge. The covalency increases with Mn doping i.e. more covalency for Mn-O bonds than Zn-O bonds. The increase in the covalency with Mn doping is confirmed by the charge density difference.

The imaginary and reel parts of the complex dielectric function are shown for ZnO and MZO (Fig. 8.a). The first peak at ~6 eV arises from electron excitation from O-*2p* state to Mn-*3d* state or Zn-*4s* state, and its

intensity remains unchanged with increasing x due to the substitution of Zn atoms by Mn atoms. The peak at ~10 eV results from electron excitation from Zn-*3d* state near VB to O-*2p* state near CB. The excitation of Zn-*3d* state to O-*2s* state induces the third strong peak at ~16 eV, which slightly decreases with increasing x due to the reduction of Zn-*3d* responsible for this transition. A slight shift toward low energy of the dielectric function is observed due to the small band gap shrinking from ZnO to MZO. The static dielectric function $\varepsilon(0)$ shows a slight change with increasing x; $\varepsilon_1(0) = 2.975$ for $x = 0$ %, 2.968 for $x = 3.7$ % (Inset in Fig. 8.a) compared to the experiment (Table 2). The complex conductivity function, complex refractive index, absorption coefficient optical reflectivity, and energy-loss function are then deduced from dielectric function (Fig. 8.b–f). The peak of the energy loss function at ~23.0 eV align with a sharp reduction in reflectivity. The absorption exhibits tow strong peaks at ~15 and 35 eV. The refractive index remains nearly constant around 1.72 with increasing *x* for lower photon energies (Inset in Fig. 8.b), which differs from experimental findings (Table 2) due to unaccounted surface morphology and thickness in the DFT-LDA + U calculations. Furthermore, both absorption coefficient and refractive index show similar trends to experimental results within the visible energy range.

4. Conclusion

This study aimed to investigate the effects of low Mn doping concentrations in ZnO thin films through both experimental and theoretical methods. The main findings are as follows:

i. Experimental Findings: All samples exhibited a polycrystalline hexagonal wurtzite phase and demonstrated a preferential orientation along the (0 0 2) axis. However, with increasing Mn doping, the diffraction peaks progressively weaken, suggesting a deterioration in the crystallinity of the samples, which also influences their properties. Specifically, it resulted in a smoother surface (rms: 45.24–30.47 nm), slight change in grain grain size (57.44–38.20 nm), lattice constants (a = b: 3.244–3.245 Å, c: 5.198–5.205 Å), average crystallite size (32–15 nm), and crystallinity. Additionally, Mn doping shifted the UV absorption edge to longer wavelengths (386–395 nm) and decreased transparency (93–54 %), likely due to oxygen vacancies and increased grain boundary density.
ii. Theoretical Findings: Mn doping slightly reduced the band gap energy, though this was enhanced using the GGA + U approach (3.379 eVfor x = 0 % and 3.267 for 3.7 %). It also affected the intensity of the imaginary part of the dielectric function, while the static refractive index remained unchanged (1.72).

CRediT authorship contribution statement

Elhadj Benrezgua: Writing – review & editing, Writing – original draft, Software, Formal analysis, Data curation. **Rabie Amari:** Software, Resources, Data curation, Conceptualization. **Ammar Boukhari:** Software, Investigation. **Djamel Allali:** Funding acquisition, Formal analysis, Data curation. **Smail Terchi:** Visualization, Formal analysis. **Abdelhamid Guellil:** Software, Resources, Project administration. **Bahri Deghfel:** Writing – original draft, Visualization, Software, Conceptualization. **Abdelhalim Zoukel:** Resources, Funding acquisition, Conceptualization. **Ahmad Azmin Mohamad:** Writing – review & editing, Validation, Project administration, Methodology, Investigation.

Declaration of competing interest

The authors declare that they have no known competing financial interests or personal relationships that could have appeared to influence the work reported in this paper.

Acknowledgements

The authors wish to thank the Algerian Ministry of Higher Education and Scientific Research represented by the Thematic Research Agency in Health and Life Sciences (TRAHLS) for financial support under the National Research Programs (NRP).

Data availability

Data will be made available on request.

References

[1] W. Chen, J. Wang, M.-R. Wang, Influence of doping concentration on the properties of ZnO: Mn thin films by sol–gel method, Vacuum 81 (2007) 894–898.
[2] G. Demircan, E.F. Gurses, B. Aktas, S. Yalcin, A. Acikgoz, G. Ceyhan, M.V. Balak, Sol–gel synthesis of Si-ZnO, Ti-ZnO and Si-Ti-ZnO thin films: impact of Si and Ti content on structural and optical properties, Mater. Today Commun. 34 (2023) 105234.
[3] E.B. Buzok, S. Yalcin, G. Demircan, D. Yılmaz, B. Aktas, E. Aytar, The structural, optical, electrical and radiation shielding properties of Co-doped ZnO thin films, Radiat. Phys. Chem. 222 (2024) 111840.
[4] G. Demircan, A. Acikgoz, S. Yalcin, E. Aytar, M.V. Balak, B. Aktas, The influence of doping perimidine ruthenium complexes on structural, optic, and residual stress properties of ZnO thin films, Braz. J. Phys. 53 (2023) 20.
[5] M. Xin, L.Z. Hu, D.-P. Liu, N.-S. Yu, Effect of Mn doping on the optical, structural and photoluminescence properties of nanostructured ZnO thin film synthesized by sol–gel technique, Superlattice. Microst. 74 (2014) 234–241.
[6] S.T. Shishiyanu, T.S. Shishiyanu, O.I. Lupan, Sensing characteristics of tin-doped ZnO thin films as NO2 gas sensor, Sens. Actuators B 107 (2005) 379–386.
[7] M.V. Gallegos, C.R. Luna, M.A. Peluso, L.C. Damonte, J.E. Sambeth, P.V. Jasen, Effect of Mn in ZnO using DFT calculations: magnetic and electronic changes, J. Alloys Compd. 795 (2019) 254–260.
[8] A. Boukhari, B. Deghfel, A. Mahroug, R. Amari, N. Selmi, S. Kheawhom, A. A. Mohamad, Thickness effect on the properties of Mn-doped ZnO thin films synthesis by sol-gel and comparison to first-principles calculations, Ceram. Int. 47 (2021) 17276–17285.
[9] S. Lany, A. Zunger, Assessment of correction methods for the band-gap problem and for finite-size effects in supercell defect calculations: case studies for ZnO and GaAs, Phys. Rev. B 78 (2008) 235104.
[10] A. Peles, GGA+ U method from first principles: application to reduction–oxidation properties in ceria-based oxides, J. Mater. Sci. 47 (2012) 7542–7548.
[11] S.L. Dudarev, G.A. Botton, S.Y. Savrasov, C. Humphreys, A.P. Sutton, Electron-energy-loss spectra and the structural stability of nickel oxide: an LSDA+ U study, Phys. Rev. B 57 (1998) 1505.
[12] J.P. Allen, G.W. Watson, Occupation matrix control of d-and f-electron localisations using DFT+ U, PCCP 16 (2014) 21016–21031.
[13] J. Silva, N.A. Neto, M. Oliveira, R. Ribeiro, S. de Lazaro, Y. Gomes, C. Paskocimas, M. Bomio, F. Motta, Recent progress and approaches on the synthesis of Mn-doped zinc oxide nanoparticles: a theoretical and experimental investigation on the photocatalytic performance, New J. Chem. 44 (2020) 8805–8812.
[14] M. Samadi, M. Zirak, A. Naseri, E. Khorashadizade, A.Z. Moshfegh, Recent progress on doped ZnO nanostructures for visible-light photocatalysis, Thin Solid Films 605 (2016) 2–19.
[15] G. Demircan, E.F. Gurses, A. Acikgoz, S. Yalcin, B. Aktas, Effects of spin coating parameters on stress, electrical and optical properties of multilayer ZnO thin film prepared by sol–gel, Mol. Cryst. Liquid Cryst. 709 (2020) 61–69.
[16] D.V. Vu, D.H. Le, T.T. Nguyen, T. Van Duong, Q.D. Ngo, T.Q. Trinh, Study on material properties of Sn-and Cu-doped ZnO thin films as n-and p-type thermoelectric materials based on wet solution synthesis, J. Mater. Sci.: Mater. Electron. 30 (2019) 6544–6551.
[17] S.J. Clark, M.D. Segall, C.J. Pickard, P.J. Hasnip, M.I. Probert, K. Refson, M. C. Payne, First principles methods using CASTEP, Zeitschrift Für Kristallographie-Crystall. Mater. 220 (2005) 567–570.
[18] J.P. Perdew, K. Burke, M. Ernzerhof, Generalized gradient approximation made simple, Phys. Rev. Lett. 77 (1996) 3865.
[19] R. Amari, B. Deghfel, A. Mahroug, A.A. Mohamad, A. Boukhari, N. Selmi, Effects of Mn doping on the structural, morphological, electronic and optical properties of ZnO thin films by sol-gel spin coating method: an experimental and DFT+ U study, Phys. B Condens. Matter 577 (2020) 411766.
[20] D. Vanderbilt, Soft self-consistent pseudopotentials in a generalized eigenvalue formalism, Phys. Rev. B 41 (1990) 7892.
[21] V.I. Anisimov, F. Aryasetiawan, A. Lichtenstein, First-principles calculations of the electronic structure and spectra of strongly correlated systems: the LDA+ U method, J. Phys. Condens. Matter 9 (1997) 767.
[22] E. Benrezgua, B. Deghfel, A. Mahroug, M.K. Yaakob, A. Boukhari, R. Amari, S. Kheawhom, A.A. Mohamad, Experimental and theoretical studies on structural, morphological, electronic, optical and magnetic properties of Zn1-xCuxO thin films ($0 \leq x \leq 0.125$), Mater. Sci. Semicond. Process. 134 (2021) 106012.
[23] A. Boukhari, B. Deghfel, A. Mahroug, R. Amari, N. Selmi, A.A. Mohamad, Thickness effect on the properties of 4% Mn-doped ZnO thin films grown by sol-gel spin

coating deposition, in: Macromolecular Symposia, Wiley Online Library, 2021, pp. 2000235.
[24] D. Shuang, X. Zhu, J. Wang, X. Zhong, G. Huang, C. He, The influence of Mn content on luminescence properties in Mn-doped ZnO films deposited by ultrasonic spray assisted chemical vapor deposition, Appl. Surf. Sci. 257 (2011) 6085–6088.
[25] R. Amari, A. Mahroug, A. Boukhari, B. Deghfel, N. Selmi, Structural, optical and luminescence properties of ZnO thin films prepared by sol-gel spin-coating method: effect of precursor concentration, Chin. Phys. Lett. 35 (2018) 016801.
[26] X. Li, X. Zhu, K. Jin, Study on structural and optical properties of Mn-doped ZnO thin films by sol-gel method, Opt. Mater. 100 (2020) 109657.
[27] M. Shatnawi, A. Alsmadi, I. Bsoul, B. Salameh, M. Mathai, G. Alnawashi, G.M. Alzoubi, F. Al-Dweri, M.J.R.P. Bawa'aneh, Influence of Mn doping on the magnetic and optical properties of ZnO nanocrystalline particles, 6 (2016) 1064-1071.
[28] S. Yang, Y. Zhang, Structural, optical and magnetic properties of Mn-doped ZnO thin films prepared by sol–gel method, J. Magn. Magn. Mater. 334 (2013) 52–58.
[29] Z.S.A. Mosa, I.M. Mohammed, T.H. Mubarak, Z.M. Abood, N.F. Habubi, S.S. Chiad, Effect of Mn-doping on optical and structural properties of ZnO thin films prepared by spray pyrolysis technique, in: AIP Conference Proceedings, AIP Publishing, 2023.
[30] N.T. Abood, P.B. Sable, G.M. Dharne, SILAR-deposited manganese doped zinc oxide thin films for NO2 gas detection applications, Phase Transit. 96 (2023) 274–289.
[31] M. Mazhdi, J. Saydi, M. Karimi, J. Seidi, F.J.O. Mazhdi, A study on optical, photoluminescence and thermoluminescence properties of ZnO and Mn doped-ZnO nanocrystalline particles, 124 (2013) 4128–4133.
[32] Y. Kim, J.-Y. Leem, Effects of precursor concentration on structural and optical properties of ZnO thin films grown on muscovite mica substrates by sol–gel spin-coating, Nanosci. Nanotechnol. 16 (2016) 5186–5189.
[33] M. DrDomenico Jr., S.J. Wemple, Oxygen-octahedra ferroelectrics. I. Theory of electro-optical and nonlinear optical effects, 40 (1969) 720–734.
[34] M. Makowiec, A. Kolek, Urbach tails in indium arsenide studied using nonequilibrium Green's functions, Phys. Rev. Appl. 22 (2024) 044053.
[35] V. Ligatchev, On nature of Urbach's tail in optical absorption spectrum of nano-crystalline zinc oxide (nc-ZnO), in: AIP Conference Proceedings, AIP Publishing, 2024.
[36] B. Sadigh, P. Erhart, D. Åberg, A. Trave, E. Schwegler, J. Bude, First-principles calculations of the Urbach tail in the optical absorption spectra of silica glass, Phys. Rev. Lett. 106 (2011) 027401.
[37] Y.J. Caglar, Compounds, sol–gel derived nanostructure undoped and cobalt doped ZnO: structural, optical and electrical studies, 560 (2013) 181–188.
[38] E.Ş. Tüzemen, S. Eker, H. Kavak, R.J.A.S.S. Esen, Dependence of film thickness on the structural and optical properties of ZnO thin films, 255 (2009) 6195–6200.
[39] M. Salem, I. Massoudi, S. Akir, Y. Litaiem, M. Gaidi, K. Khirouni, Photoelectrochemical and opto-electronic properties tuning of ZnO films: effect of Cu doping content, J. Alloys Compd. 722 (2017) 313–320.
[40] W. Oo, L.V. Saraf, M.H. Engelhard, V. Shutthanandan, L. Bergman, J. Huso, M. D. Mccluskey, Suppression of conductivity in Mn-doped ZnO thin films, J. Appl. Phys. 105 (2009).
[41] K. Harun, N.A. Salleh, B. Deghfel, M.K. Yaakob, A.A. Mohamad, DFT+ U calculations for electronic, structural, and optical properties of ZnO wurtzite structure: a review, Results Phys. 16 (2020) 102829.
[42] A. Ciechan, P.J.O.M. Bogusławski, Transition metal ions in ZnO: effects of intrashell coulomb repulsion on electronic properties, 79 (2018) 264–268.